Fountains impinging on a density interface

JOSEPH K. ANSONG[1], PATRICK J. KYBA[1] AND BRUCE R. SUTHERLAND[2]

[1]Department of Mathematical and Statistical Sciences, University of Alberta,
Edmonton, AB, Canada T6G 2G1

[2]Departments of Physics and of Earth and Atmospheric Sciences, University of Alberta,
Edmonton, AB, Canada T6G 2G7

We present an experimental study of an axisymmetric turbulent fountain in a two-layer stratified environment. Interacting with the interface, the fountain is observed to exhibit three regimes of flow. It may penetrate the interface, but nonetheless return to the source where it spreads as a radially propagating gravity current; the return flow may be trapped at the interface where it spreads as a radially propagating intrusion or it may do both. These regimes have been classified using empirically determined regime parameters which govern the relative initial momentum of the fountain and the relative density difference of the fountain and the ambient fluid. The maximum vertical distance travelled by the fountain in a two-layer fluid has been theoretically determined by extending the theory developed for fountains in a homogeneous environment. The theory compares favourably with experimental measurements. We have also developed a theory to analyse the initial speeds of the resulting radial currents. The spreading currents exhibited two different flow regimes: a constant-velocity regime and an inertia-buoyancy regime in which the front position, R, scales with time, t, as $R \sim t^{3/4}$. These regimes were classified using a critical Froude number which characterized the competing effects of momentum and buoyancy in the currents.

1. Introduction

Turbulent forced plumes in both homogeneous and stably stratified ambient fluids have received considerable attention, in part owing to their environmental impact in such areas as the disposal of sewage in the ocean and in lakes, volcanic eruptions into the atmosphere and emissions from chimneys and flares. The dynamics of plumes and fountains in enclosed spaces have been studied in order to improve the efficiency through which rooms are heated and cooled (Lin & Linden 2005*a*).

Forced plumes are characterized by the competing effects of buoyancy and momentum in the flow. In positively buoyant plumes, the buoyancy and momentum are both in the same direction with buoyancy becoming more dominant at larger distances away from the source. Negatively buoyant plumes, or fountains, are formed either when dense fluid is continuously discharged upward into a less dense fluid or when less dense fluid is injected downward into a more dense environment. In either case, buoyancy opposes the momentum of the flow until the fountain reaches a height where the vertical velocity goes to zero. The fountain then reverses direction and falls back upon the source.

Positively and negatively buoyant plumes have been examined theoretically and experimentally as they evolve in homogeneous and in linearly stratified environments (Priestley & Ball 1955; Morton 1959*b*; Turner 1966; Abraham 1963; Fischer *et al.* 1979; List 1982; Rodi 1982; Bloomfield & Kerr 1998; Bloomfield & Kerr 2000). Most of this effort was directed at quantifying the width of the fountain, the initial and final heights (or penetration depths) and the entrainment into the fountain.

Fountains in a two-layer stably stratified environment have received relatively little attention despite their fundamental nature and their potential practical significance. A ventilated room can naturally form a two layer-stratification and it is of interest to know how cold air injected from below mixes in this environment. Jets and fountains in two-layer ambient have also been reported in the situation of refuelling compensated fuel tanks on naval vessels (Friedman & Katz 2000). The thermocline in lakes and oceans and atmospheric inversions can be modelled approximately as the interface of a two-layer fluid (Mellor 1996), and plumes and fountains can result from the release of effluent into these environments (Rawn, Bowerman & Brooks 1960; Noutsopoulos & Nanou 1986).

This work is, in part, the first stage of a programme to understand the evolution of pollutants from flares that disperse in the presence of an atmospheric inversion. Atmospheric inversions, known for their strong vertical stability, can trap air pollutants below or within them near ground level and so have adverse effects on human health. Hazardous industrial materials that are released into the atmosphere usually form clouds that are heavier than the atmosphere (Britter 1989). Both Morton (1959*a*) and Scorer (1959) have applied available mathematical concepts of plume theory to study the dispersion of pollutants in the atmosphere, but ignored the effects of an inversion.

Here we present an experimental study of an axisymmetric fountain impinging on a density interface in a two-layer stably stratified environment. As in homogeneous environments, the fountain comes to rest at a maximum height and then reverses direction, interacting with the incident flow.

In a two-layer fluid, however, the reverse flow can either return to the level of the source or it can become trapped at the density interface. In either case, the return flow then goes on to spread radially outward. We wish to develop a better understanding of the flow through measurements of maximum penetration height, quasi-steady-state height and radial spreading rate.

There are few experimental studies on fountains in a two-layer environment. Kapoor & Jaluria (1993) considered a two-dimensional fountain in a two-layer thermally stratified ambient. They provided empirical formulae for the penetration depths in terms of a defined Richardson number.

Some have considered a jet directed into a two-layer ambient with the initial density of the jet being the same as the density of the ambient at the source (Shy 1995; Friedman & Katz 2000 and Lin & Linden 2005*b*). Those jets only become negatively buoyant in the second layer.

Noutsopoulos & Nanou (1986) studied the upward discharge of a buoyant plume into a two-layer stratified ambient and used a stratification parameter that depended on the density differences in the flow to analyse their results.

One outstanding question concerns whether the reverse flow has a significant effect on the axial velocity and density. By measuring temperatures in a heated turbulent air jet discharged downward into an air environment, Seban, Behnia & Abreu (1978) showed that the centreline temperatures and the penetration depth can be predicted well by theories which consider the downward flow alone. Mizushina *et al.* (1982) made a similar study of fountains by discharging cold water upward into an environment

of heated water and found that the reverse flow had an effect on the axial velocity measurements. They attributed the difference in their result from those of Seban *et al.* (1978) to the enclosure used by Seban *et al.* in their experiments.

These experimental results have served to improve only modestly our understanding of the dynamics of the reverse flow. A theoretical study aimed at incorporating the reverse flow was first undertaken by McDougall (1981) who developed a set of entrainment equations quantifying the mixing that occurs in the whole fountain. The ideas developed in the model of McDougall (1981) have been built upon by Bloomfield & Kerr (2000) by considering an alternative formulation for the entrainment between the upflow and the downflow. Their results for the width of the whole fountain, the centreline velocity and temperature compared favourably with the experiments of Mizushina *et al.* (1982).

An important requirement for studying the dispersion of dense gases in the atmosphere is a knowledge of the distribution of the density as a function of space and time (Britter 1989) and how fast the spreading pollutants are moving from a particular location. The usual approach to obtaining information on fluid densities in experiments is by extracting samples from the flow. This is difficult and has led to the introduction of a relatively new approach of laser-induced fluorescence (LIF). This is, however, limited to unstratified environments owing to problems with refractive index fluctuations (Daviero, Roberts & Mile 2001). In this study, we do not take measurements of the densities of the spreading currents, but we focus on taking measurements of the initial speeds of the radial currents as they spread from the area of impingement.

In §2, we review the theory for fountains in a one-layer environment and extend it to the two-layer case. In §3, we develop the theory for the axisymmetric spreading of currents from fountains. In §4, we describe the set-up of the laboratory experiments and the techniques used to visualize the experiments, and we present their qualitative analyses. In §5, quantitative results from the experiments are presented. We analyse the classification of the regimes of flow and compare the measured maximum penetration height and spreading velocities to theoretical predictions. In §6, we summarize the results.

2. Theory: penetration height

The following theory is developed for fountains in which heavier fluid is injected upward into a less dense environment. However, in a Boussinesq fluid, for which the density variations are small compared with the characteristic density, the direction of motion is immaterial to the equations governing their dynamics.

2.1. *The maximum height in a one-layer ambient*

The conventional and most widely used approach to solving problems of turbulent buoyant jets is to use the conservation equations of turbulent flow of an incompressible fluid and employ the Boussinesq and boundary-layer approximations. The resulting equations are typically solved by using the Eulerian integral method (Turner 1973). Here a form is first assumed for the velocity and concentration profiles of the plume. This could either be the Gaussian profile or the top-hat profile. The equations are then integrated over the plume cross-section and the assumed profiles are substituted. The result is three ordinary differential equations (ODEs) which may be solved analytically or numerically. However, an assumption has to be made to close the system of ODEs. This could either be the entrainment assumption introduced by Morton, Taylor & Turner (1956), or the spreading assumption introduced by Abraham (1963).

A detailed description of the internal structure of the fountain can be found in Abraham (1963) where the solution approach leads to a division of the fountain into four zones: a zone of flow establishment where the fountain initially acts like a jet; a zone of established flow where the flow is considered to be fully established and permits the assumption of self-similarity; a zone of positive entrainment where the fountain entrains fluid from the environment; and a zone of negative entrainment (close to the maximum height) where the fountain does not entrain fluid from the ambient, but begins to return toward the source.

When the fountain reverses direction from the maximum height, the rising upward flow then entrains fluid from the downflow and vice versa and also continues to entrain fluid from the environment until the fountain collapses at the level of the source. It is difficult to ascertain the amount of the mixed fluid entrained into the fountain, and the theoretical approach mentioned above treats the problem as if only the ambient fluid is entrained.

An alternative approach is the Lagrangian method in which a marked material volume issuing from a plume source is followed in time (Baines & Chu 1996; Lee & Chu 2003). The solutions are much simpler to obtain and interpret and they give very good agreement with the Eulerian integral method.

We give a brief review of the Lagrangian method for a fountain in a uniform ambient. Newton's law is applied to a material volume such that the rate of change of the vertical momentum of the plume element is equal to the buoyancy force:

$$\frac{\mathrm{d}M}{\mathrm{d}t} = -F_0, \tag{2.1}$$

where M and F_0 are the momentum flux per unit mass and the buoyancy flux, respectively. Explicitly, assuming a top-hat-shaped plume of radius r and mean vertical velocity w, $M = \pi r^2 w^2$ and $F_0 = \pi r_0^2 w_0 g'$, in which $g' = (\rho_a - \rho)g/\rho_0$ is the reduced gravity, r_0 is the source radius, w_0 is the average vertical velocity at the source, ρ_a is the ambient density, ρ is the density of the fountain at a given height and ρ_0 is a reference density taken as the initial density of the fountain. We apply the spreading hypothesis which assumes that $\mathrm{d}r/\mathrm{d}z = \beta$, where β is a constant spreading coefficient ($\beta \approx 0.17$, Baines & Chu 1996). The buoyancy flux F_0 is constant in a uniform ambient. Thus we obtain the following relations for the radius, r, height, z, volume flux, $Q = \pi r^2 w$, and momentum flux, M, of the fountain as a function of time, t:

$$r = \left(\frac{4\beta}{3\sqrt{\pi}}\right)^{1/2} \frac{M_0^{3/4}}{F_0^{1/2}} \left[1 - \left(1 - \frac{F_0 t}{M_0}\right)^{3/2}\right]^{1/2}, \tag{2.2}$$

$$z = \left(\frac{4}{3\beta\sqrt{\pi}}\right)^{1/2} \frac{M_0^{3/4}}{F_0^{1/2}} \left[1 - \left(1 - \frac{F_0 t}{M_0}\right)^{3/2}\right]^{1/2}, \tag{2.3}$$

$$Q = M_0^{1/2} \left(\frac{4\beta\sqrt{\pi}}{3}\right) \frac{M_0^{3/4}}{F_0^{1/2}} \left(1 - \frac{F_0 t}{M_0}\right)^{1/2} \left[1 - \left(1 - \frac{F_0 t}{M_0}\right)^{3/2}\right]^{1/2}, \tag{2.4}$$

$$M = M_0 - F_0 t, \tag{2.5}$$

in which $M_0 = \pi r_0^2 w_0^2$ is the momentum flux per unit mass at the source. Equations (2.2)–(2.5) were derived assuming a point source of flow; nevertheless, they could also be derived for any given source radius. At the maximum height, the momentum flux goes to zero, so that from (2.5) we obtain the time taken to reach the maximum

height as

$$t_{max} = \frac{M_0}{F_0}. \tag{2.6}$$

Substituting (2.6) into (2.3), we obtain the maximum penetration height of the fountain:

$$z_{max} = C_f \frac{M_0^{3/4}}{F_0^{1/2}}, \tag{2.7}$$

where $C_f = (4/3\beta\sqrt{\pi})^{1/2} \approx 2.10$. This formula was also obtained by Turner (1966) through dimensional considerations.

Equation (2.7) may be rewritten in terms of the source Froude number, $Fr_0 = w_0/\sqrt{g'r_0}$, such that

$$z_{max} = Cr_0 Fr_0, \tag{2.8}$$

in which $C = \sqrt{8/(3\beta)} \approx 3.96$. As expected, (2.4) predicts that the volume flux decreases toward zero at the maximum height, indicating a negative entrainment at the region where the fountain fluid begins to fall toward the source. This also means that there is a critical time when the volume flux is maximum. This critical time, t_c, can be explicitly calculated by differentiating (2.4) with respect to t and setting the resulting expression to zero to obtain:

$$t_c = \frac{M_0}{F_0} \left[1 - \left(\frac{2}{5} \right)^{2/3} \right]. \tag{2.9}$$

Substituting t_c into (2.4) gives the maximum volume flux:

$$Q_{max} = M_0^{1/2} \sqrt{\pi} \left(\frac{4\beta}{3\sqrt{\pi}} \right)^{1/2} \frac{M_0^{3/4}}{F_0^{1/2}} \left(\frac{3}{5} \right)^{1/2} \left(\frac{2}{5} \right)^{1/3}. \tag{2.10}$$

Before reaching the maximum height, conservation of buoyancy flux implies that the density of the fountain can be calculated at each height once the volume flux is known:

$$Q_0 g_0' = Q g',$$
$$\implies \rho = \rho_a - \frac{Q_0}{Q}(\rho_a - \rho_0). \tag{2.11}$$

However, since the volume flux reduces to zero at the maximum height, Q in (2.11) must be replaced by Q_{max} to calculate the density at the maximum height. This is because the density will remain unchanged from t_c to t_{max} owing to the negative entrainment in this region.

Upon reaching the maximum height, the fountain reverses direction interacting with the incident flow. The interaction between these two opposing fluids inhibits the rise of the incident flow to the initial height and so it settles at a quasi-steady-state height, z_{ss}. The theory above cannot be used to predict the final height; however, experimental measurements show that $z_{ss} \approx 0.70 z_{max}$ (Turner 1966).

The return flow continues to fall while entraining fluid from the environment and the upward flow until it reaches the level of the source where it redirects from a vertical flow to a radial current. There are no experimental studies on these radial currents. However, it has been observed that the height of the radial currents is proportional to the maximum height (Baines, Turner & Campbell 1990).
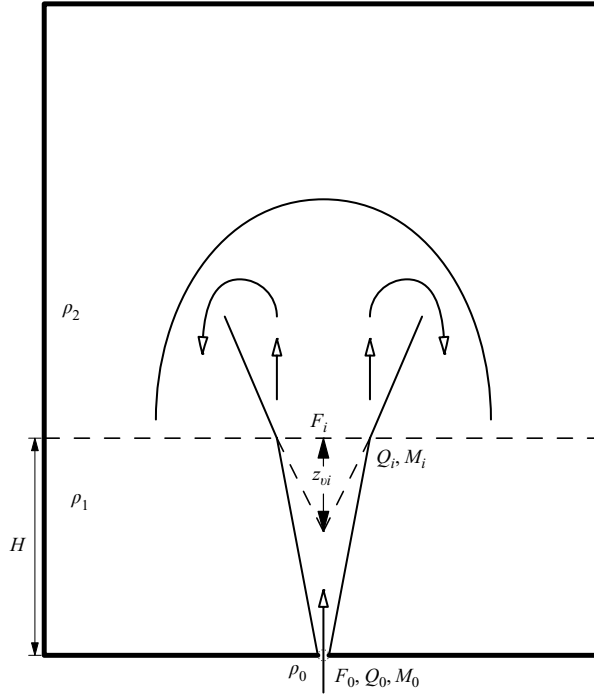
FIGURE 1. Schematic of a fountain in a two-layer ambient.

2.2. The maximum height in a two-layer ambient

To obtain the maximum height in a two-layer ambient, we first calculate the centreline fluxes of the upward-moving fluid at the interface using (2.2)–(2.5) (see figure 1). Then we calculate the buoyancy flux, F_i, of the fountain above the interface, using the approach of Noutsopoulos & Nanou (1986). Noutsopoulos & Nanou (1986) obtained the nominal value of the buoyancy flux above the interface as

$$F_i = \frac{1}{\rho_0} \int_A g(\rho_2 - \rho)w \, \mathrm{d}A = g\frac{(\rho_1 - \rho_0)}{\rho_0}Q_0 - g\frac{(\rho_1 - \rho_2)}{\rho_0}Q_i = F_0 \left[1 - \tilde{\varepsilon}\frac{Q_i}{Q_0}\right],$$

where $Q_i = \pi r_i^2 w_i$ is the volume flux, r_i is the radius and w_i is the velocity of the fountain at the interface, and $\tilde{\varepsilon} = (\rho_1 - \rho_2)/(\rho_1 - \rho_0)$. Finally, using F_i, we calculate the depth of the virtual origin below the interface, z_{vi}, following the method of Morton (1959b) (see Appendix A). This approach results in the following formula for the maximum height

$$z_{max,2} = H + Cr_i Fr_i - z_{vi}, \tag{2.12}$$

where $Fr_i = w_i / \sqrt{g(\rho_2 - \rho_i)r_i/\rho_0}$, ρ_i is the density of the fountain at the interface and H is the distance of the source from the interface.

The second and third terms in (2.12) estimate the maximum height of the fountain from the interface. If the fountain penetrates little beyond the interface, the second term may be less than z_{vi}. The best estimate for the maximum height in such a case should be $z_{max,2} \approx H$. The buoyancy flux above the interface may also be obtained as $F_i = g'_{bi}Q_i$, where $g'_{bi} = g(\rho_2 - \rho_i)/\rho_0$ is the reduced gravity of the fountain at the interface.

The procedure above assumes that the density difference between the layers is small and considers the fountain from the interface as one moving in a one-layer environment. The constant-spreading assumption may therefore be used in this instance since the spreading rate of the fountain in the top layer as depicted in figure 1 is exaggerated only to illustrate the theoretical procedure. Our experiments show that the fountain penetrates the interface without a noticeable change in structure (see §4.2.2).

In this paper, we will also test the theoretical solution of Abraham (1963) who obtained the following approximate analytic solution for the penetration of a turbulent buoyant jet moving into an environment consisting of two layers of different densities:

$$z_{max,2} = \left(\tfrac{2}{5}\right)^{1/6} \left(\tfrac{3}{2} - \mu \tilde{F}\right)^{1/2} H, \qquad (2.13)$$

in which $\tilde{F} = w_i^2/((\rho_i - \rho_2)gH/\rho_0)$ and the empirical constant $\mu \approx 0.8$ (Abraham 1963). This derivation assumed Gaussian profiles of the flow quantities, unlike the top-hat approach considered in this study.

Similar to the one-layer case, the interaction of the incident and reverse flows inhibits the incident flow from reaching the maximum height and thus settles at a quasi-steady-state height, $z_{ss,2}$. Unlike the one-layer case, the return flow may intrude on the interface or continue to the level of the source. Our experiments show that the ratio of the steady-state height to the maximum height depends on whether the return flow went back to the source or collapsed at the interface (see §5.2 where we have also compared our results with those of Bloomfield & Kerr 1998).

The most significant factors governing these flow regimes are the relative density differences between the two layers and fountain and the maximum height relative to the height, H, of the layer at the source. Explicitly, the relative density differences are characterized by

$$\theta = \left| \frac{\rho_2 - \rho_1}{\rho_2 - \rho_0} \right|, \qquad (2.14)$$

and the relative maximum height is characterized by z_{max}/H.

$\theta = 0$ if $\rho_2 = \rho_1$, in which case the ambient is a one-layer fluid and the fountain must return to the source. The same circumstance is expected if $z_{max} < H$ since the fountain does not reach the position of the interface.

$\theta = 1$ if $\rho_1 = \rho_0$, in which case the flow does not act like a fountain until impacting the second layer. No experiments were conducted for this case, but the interested reader may refer to Shy (1995), Friedman & Katz (2000) and Lin & Linden (2005b). If the jet penetrates the interface ($z_{max} > H$), the resulting fountain will be expected to return to spread along the interface since the fountain entrains less dense fluid from beyond the interface and therefore becomes lighter than the ambient fluid at the source.

Irrespective of the regime that occurs, the flow goes on to spread as a radial current.

3. Theory: spreading velocities

In the following, we derive a theory to analyse the velocities of the spreading currents at the source and the interfacial intrusions. We consider only the radial velocities at the radius of the whole fountain where the return flow redirects from a vertical to a horizontal flow.
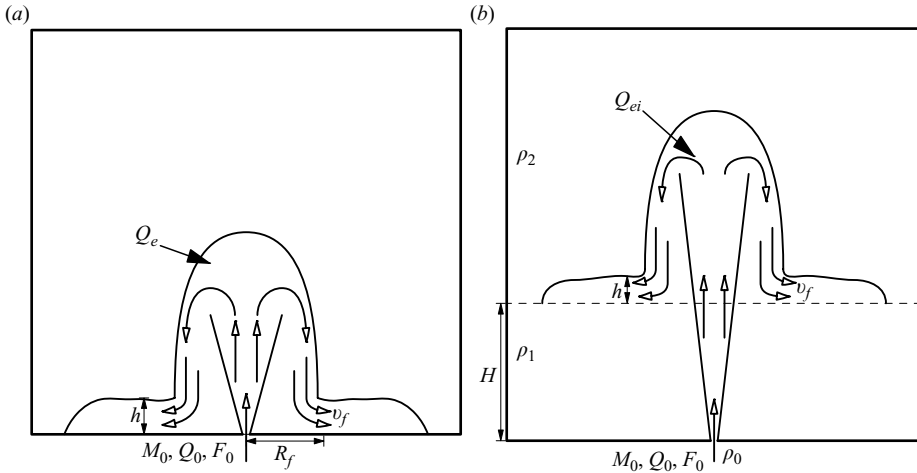
FIGURE 2. Schematics of (*a*) one-layer surface spreading currents, and (*b*) a model of the interfacial spreading currents.

There are three cases to be considered. We first consider the theory for the spreading velocities of the currents at the source in the one-layer case and then extend it to examine source-spreading of fountains in two-layer fluids. The velocities of radial intrusions at the interface of a two-layer fluid is considered as a third case.

3.1. *Case 1: one-layer source-spreading*

Figure 2(*a*) is a schematic showing the spreading of the currents at the source from a fountain in a one-layer environment. Baines *et al.* (1990) modelled the return flow of a turbulent fountain as an annular plane plume and obtained a formula for the total lateral entrainment into the reverse flow as

$$Q_e = B \frac{(z_{max} - z_v)}{r_0} Q_0, \tag{3.1}$$

where $B \approx 0.25$ was obtained as an experimental constant and z_v is the distance of the virtual origin below the source ($z_v \approx 0.8$ cm for our experiments). Thus, the total volume flux at the level of the source, just as the flow begins to spread outward is given by

$$Q_T = Q_e + Q_0. \tag{3.2}$$

If v_f is the initial spreading velocity at a radial distance R_f, where R_f is the radius of the return flow at the source, and h is the corresponding height of the spreading layer just as the currents enter the ambient, then

$$Q_T = 2\pi R_f h v_f. \tag{3.3}$$

Defining $g'_T = g(\rho_1 - \rho_s)/\rho_s$ to be the reduced gravity and ρ_s to be the initial density of the spreading layer at $r = R_f$, dimensional analysis gives, for a buoyancy-driven flow, a relationship of the form $v_f \propto \sqrt{g'_T h}$. Using (3.3), we obtain

$$v_f \propto \left(\frac{Q_T g'_T}{R_f} \right)^{1/3}. \tag{3.4}$$

Mizushina *et al.* (1982) show that the radius of the whole fountain is approximately constant and is about 22 % of the quasi-steady state height, z_{ss}. Just before the return

flow begins to spread into the ambient, conservation of buoyancy flux in the fountain requires that at the level of the source

$$g'_T(Q_e + Q_0) = g'_e Q_e + g'_0 Q_0, \tag{3.5}$$
$$\Rightarrow g'_T Q_T = F_0, \tag{3.6}$$

since by definition the reduced gravity of the environment, g'_e, is zero. Thus, from (3.4) and (3.6) we obtain

$$v_f \propto \left(\frac{F_0}{R_f}\right)^{1/3} \propto \left(\frac{F_0}{z_{ss}}\right)^{1/3}. \tag{3.7}$$

This formula may also be obtained via scaling analysis. By balancing the driving buoyancy force which scales as $g'_T \rho_s R h^2$, and the retarding inertia force which scales as $\rho_s h R^3/t^2$, Chen (1980) obtained the position of the front, R, as a function of time, t, as $R(t) = c F_0^{1/4} t^{3/4}$ (where $c = 0.84$ was obtained as an experimental constant), thus the velocity, v, is given by

$$v = \frac{\mathrm{d}R}{\mathrm{d}t} = 0.59 \left(\frac{F_0}{R}\right)^{1/3}, \tag{3.8}$$

where the global volume conservation relation, $Q_T t = \pi R^2 h$, has been employed. The same power law behaviour was also obtained by Britter (1979) by solving the governing equations of motion and obtained the experimental constant $c = 0.75$.

The scaling relationships above assume that the flow is a pure gravity current, its motion being dominated by buoyancy forces. In the presence of substantial radial momentum at the point where the flow enters the environment, dimensional analysis shows that at small times compared with the characteristic time scale $t_{MF} = M_R/F_R$ (in which M_R is the radial component of momentum flux per unit mass and F_R is the radial buoyancy flux per unit mass), the flow is dominated by momentum such that $R(t) \sim M_R^{1/4} t^{1/2}$ (Chen 1980), so that

$$v \sim M_R^{1/2}/R. \tag{3.9}$$

Kotsovinos (2000) showed a contant-velocity regime where $R \sim t$ for contant-flux axisymmetric intrusions into a linearly stratified ambient. Kotsovinos argued that the additional force driving the flow in such cases is the initial radial momentum flux $(\rho_s M_R)$. Thus, balancing the kinematic momentum flux and the rate of change of the inertia force which scales as $\rho_s h R^3/t^2$, gives $R(t) \sim (M_R/Q_T)t$, so that

$$v \sim M_R/Q_T. \tag{3.10}$$

In theory, the relations in (3.7) and (3.8) correspond to larger times within the inertia–buoyancy regime when the flow is purely driven by buoyancy.

The radial component of momentum is unknown *a priori*; however, owing to the loss in momentum by moving from a vertical flow to a radial current, we assume that the initial radial momentum flux, M_R, is proportional to the momentum flux of the return flow at the level of the source, M_{ret}, and defined as

$$M_{ret} = \pi (R_f^2 - r_0^2) w_{ret}^2, \tag{3.11}$$

where w_{ret} is the velocity of the return flow at the level of the source. The results of Bloomfield & Kerr (2000) show that the reverse flow of the fountain moving back toward the source first accelerates to some height before settling to an almost constant

velocity close to the source. Their results also suggest that at the source, the velocity of the return flow is such that

$$w_{ret} \propto M_0^{-1/4} F_0^{1/2}. \tag{3.12}$$

In summary, if the radial momentum of the initial flow is substantial, then three regimes are theoretically possible. These are the radial-jet regime where $R \sim t^{1/2}$, the constant-velocity regime where $R \sim t$ and the inertia–buoyancy regime where $R \sim t^{3/4}$. Thus, from (3.9), (3.10) and (3.7), and replacing M_R by M_{ret}, we obtain the following relations which may be used to predict the initial velocity of the spreading currents just as the flow begins to spread into the ambient:

$$v_{t \ll t_{MF}} \propto \left(M_{ret}^{1/2} / z_{ss} \right), \tag{3.13}$$

$$v_{t \approx t_{MF}} \propto \left(M_{ret} / Q_T \right), \tag{3.14}$$

$$v_{t \gg t_{MF}} \propto \left(F_0 / z_{ss} \right)^{1/3}. \tag{3.15}$$

However, not all three regimes are necessarily present in a single experiment; the presence of a particular regime largely depends on the competing effects of the radial components of momentum and buoyancy in the flow (Chen 1980; Kotsovinos 2000).

3.2. Case 2: two-layer surface-spreading

We consider the case where the return flow in the two-layer case returns to spread at the source as an axisymmetric current. In this case, there are two buoyancy fluxes involved in the system: the initial buoyancy flux, F_0, and the buoyancy flux after the fountain penetrates the density interface, F_i. The total volume flux of the spreading layer is given by the sum of the volume fluxes at the source and the interface, and the flux entrained from the environment:

$$Q_{st} = Q_e + Q_0 + Q_i,$$

where z_{max} in (3.1) is now replaced by $z_{max,2}$. The spreading layer will consist of a mixture of the source fluid and the fluid from the bottom and top layers. The mixture of fluid determines the reduced gravity of the spreading layer such that

$$g'_{st}(Q_e + Q_0 + Q_i) = g'_e Q_e + g'_0 Q_0 + g'_{bi} Q_i,$$
$$\Rightarrow g'_{st} Q_{st} = F_0 + F_i, \tag{3.16}$$

where $g'_{st} = g(\rho_{st} - \rho_1)/\rho_{st}$ is the reduced gravity and ρ_{st} is the initial density of the spreading layer. Following the analyses in the one-layer case, we obtain the spreading velocity for a buoyancy-driven flow as

$$v_{t \gg t_{MF}} \propto \left(\frac{g'_{st} Q_{st}}{z_{ss,2}} \right)^{1/3} \propto \left(\frac{F_0 + F_i}{z_{ss,2}} \right)^{1/3}, \tag{3.17}$$

where $z_{ss,2}$ is the steady-state height in the two-layer case.

We assume that the velocity and momentum of the return flow at the level of the source are proportional to the corresponding velocity and momentum in the one-layer case where the ambient fluid is the first-layer fluid. As such, if the initial radial momentum flux is substantial, then (3.13) and (3.14) may still be applied. By replacing M_R with M_{ret}, this argument results in the velocity relations for the radial-jet and constant-velocity regimes, respectively, as

$$v_{t \ll t_{MF}} \propto \left(M_{ret}^{1/2} / z_{ss,2} \right), \tag{3.18}$$

$$v_{t \approx t_{MF}} \propto \left(M_{ret} / Q_{st} \right). \tag{3.19}$$

3.3. *Case 3: two-layer interfacial-spreading*

Experiments on axisymmetric intrusions into two-layer ambients from a source of constant volume flux are limited in the literature. Lister & Kerr (1989) have considered the case of the spreading of highly viscous fluid into a two-layer environment. They employed both scaling analysis and lubrication theory to analyse their results. Timothy (1977) considered the general case of a stratified inflow into a stratified ambient and treated the two-layer case as a special circumstance. Most of his results were derived by extending the Bernoulli and hydrostatic equations for two-dimensional rectilinear flows to axisymmetric flows.

We show in Appendix B that by balancing the horizontal driving buoyancy force and the retarding inertia force, for a buoyancy-driven flow, we obtain the relation for the radial velocity of the intrusion as

$$v \propto \left(\frac{\varepsilon g'_{in} Q_{in}}{R} \right)^{1/3}, \tag{3.20}$$

where $\varepsilon = (\rho_2 - \rho_{in})/(\rho_2 - \rho_1)$. The reduced gravity of the intrusion in this case is modified by the parameter ε. If the density of the intrusion is equal to the density of the first-layer fluid ($\rho_{in} = \rho_1$), then the one-layer relation (3.8) is retrieved from (3.20).

To model the case of the intrusions, we consider the fountain beyond the interface as though it is a one-layer system with the source conditions replaced by the conditions at the interface (see figure 2*b*). The volume flux entrained from the environment into the return flow is now given by:

$$Q_{ei} = B \frac{(z_{max,2} - H - z_v)}{r_i} Q_i,$$

and the total volume flux into the spreading layer is given by the sum of the fluxes at the source and the interface, and the flux entrained from the environment:

$$Q_{in} = Q_{ei} + Q_0 + Q_i.$$

The mixture of fluid determines the reduced gravity of the interfacial intrusions, and assuming the conservation of buoyancy relation $\varepsilon g'_{in} Q_{in} = F_0 + F_i$, we find the same proportionality relationship as in (3.17), although the proportionality constant is different:

$$v_{t \gg t_{MF}} \propto \left(\frac{F_0 + F_i}{R_f} \right)^{1/3} \propto \left(\frac{F_0 + F_i}{z_{ss,2}} \right)^{1/3}. \tag{3.21}$$

In the presence of a substantial radial component of momentum, (3.13) and (3.14) may be applied with the initial source conditions replaced by the conditions at the interface. This gives the velocity formulae for the radial-jet and constant-velocity regimes, respectively, as

$$v_{t \ll t_{MF}} \propto M_{ret,i}^{1/2} / z_{ss,2}, \tag{3.22}$$

$$v_{t \approx t_{MF}} \propto M_{ret,i} / Q_{in}, \tag{3.23}$$

where $M_{ret,i}$ is the vertical momentum of the return flow at the interface and defined as $M_{ret,i} = \pi (R_f^2 - r_i^2) w_{ret,i}^2$ with $w_{ret,i} \propto M_i^{-1/4} F_i^{1/2}$, where $w_{ret,i}$ is the velocity of the return flow at the interface.
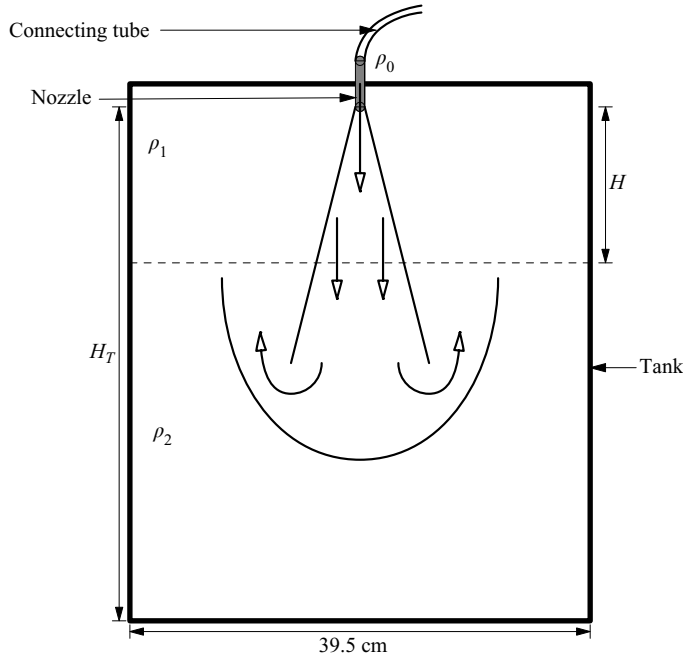
FIGURE 3. Experimental set-up and definition of parameters.

4. Experimental set-up and analyses

4.1. *Experimental set-up*

Experiments were performed in an acrylic tank measuring 39.5 cm long by 39.5 cm wide by 39.5 cm high (see figure 3). The experiments were conducted by injecting less dense fluid downward into more dense ambient fluid; however, the direction of motion is immaterial to the equations governing their dynamics since the fluid is considered to be Boussinesq. A control experiment was conducted in a one-layer homogeneous environment and 48 experiments were conducted in a two-layer fluid. In all experiments, the total depth of fluid within the tank was $H_T = 38$ cm. The tank was filled to a depth of $H_T - H$ with fluid of density ρ_2, where $H = 0$ in the case of the one-layer experiment and $H = 5$ cm or 10 cm in two-layer experiments. In two-layer experiments, a layer of fluid with density ρ_1 was added through a sponge float until the total depth was H_T. The variations in density were created using sodium chloride. The typical interface thickness between the two layers was 1 cm, sufficiently small to be considered negligible.

After the one- or two-layer fluid in the tank was established, a constant-head reservoir of fresh water of density ρ_0 was dyed with a blue food colouring and then allowed to drain into the tank through a round nozzle of radius 0.2 cm. To ensure the flow leaves the nozzle turbulently, the nozzle was specially designed and fitted with a mesh having openings of extent 0.05 cm. The flow was assumed to leave at a uniform velocity across the diameter of the nozzle. The flow rates for the experiments were recorded using a flow meter connected to a plastic tube, and by measuring the total volume released during an experiment. Flow rates ranged from 2.82 to 3.35 cm^3 s^{-1}, and the Reynolds number of the experiments, defined as $R_e = wD/\nu$, ranged from 896 to 1066, where ν is the kinematic viscosity of water, and $D = 2r_0$.

Experiments were recorded using a digital camera situated 250 cm from the front of the tank. The camera was situated at a level parallel to the mid-depth of the tank

and the entire tank was in its field of view. A fluorescent lighting apparatus was also placed about 10 cm behind the tank to illuminate the system.

Using 'DigImage' software, the maximum penetration depth of the fountain, the quasi-steady-state depth and the initial velocity, w_0, were determined by taking vertical time series constructed from vertical slices through the nozzle. The temporal resolution was as small as 1/30 s and the spatial resolution was about 0.1 cm.

Horizontal time series were used to determine the velocity of the resulting spreading currents. They were taken at a position immediately below the nozzle. Most time series are symmetrical about the position of the nozzle and only one side is used for the calculation of the velocities. Asymmetry in the time series may arise owing to instabilities in the flow causing the front of the fountain at the maximum depth to tilt to one side. These experiments were excluded from the analyses.

4.2. Qualitative results

We present in this section the qualitative results of the laboratory experiments before giving detailed analyses of them. The snapshots from the experiments are flipped upside down for conceptual convenience and for consistency with the theory. We will first describe the results of the one-layer experiment before proceeding to the two-layer case.

4.2.1. One-layer experiment

Figures 4(a) to 4(d) show snapshots of the one-layer experiment which were taken 1, 3, 5 and 8 s, respectively, after the experiment started. The density difference between the fountain and the ambient fluid was $|\rho_0 - \rho_1| = 0.0242 \, \text{g cm}^{-3}$ and the initial velocity was $w_0 = 24.3 \, \text{cm s}^{-1}$. We observe the characteristic widening of the fountain as it entrains fluid from the surrounding homogeneous fluid. It reaches its maximum height at $t \sim 1$ s (figure 4a), at which time the top of the fountain forms a pointed shape before collapsing back toward the source. The front then broadens and spreads outward as it returns downward forming a curtain around the incident upward flow (figure 4b). The interaction of the return flow with the main upflow inhibits the rise of fluid from the source and causes the fountain to settle at a quasi-steady-state height which is moderately below the maximum height. When the return flow reaches the level of the source, it begins to spread radially outward (figure 4c). The spreading layer then propagates radially away from the source (figure 4d). The experiment is stopped before the spreading layer reaches the sidewalls of the tank.

Figure 5(a) shows the horizontal time series taken from this experiment, illustrating the spreading of the surface flow on both sides of the nozzle (situated at $x = 0$ cm). The parabolic nature of the time series indicates the change in speed of the current as it moves away from the source.

Figure 5(b) shows the vertical time series taken for this experiment, and illustrates the positions of the maximum height, z_{max}, and the steady-state height, z_{ss}. The value of the ratio z_{ss}/z_{max} was found to be 0.74 for this experiment, comparable to the average value of 0.7 obtained by Turner (1966). The height of the spreading layer was observed to be almost constant as it spreads into the ambient (not shown), and was observed to be proportional to z_{max} (Baines *et al.* 1990).

4.2.2. Two-layer experiments

In the presence of a two-layer ambient, the return flow of a fountain may go back to the level of the source or it may mix sufficiently with the second layer so that it goes back to the interface. In some circumstances, it may do both. Here, only snapshots for a situation leading to interfacial intrusions are shown.
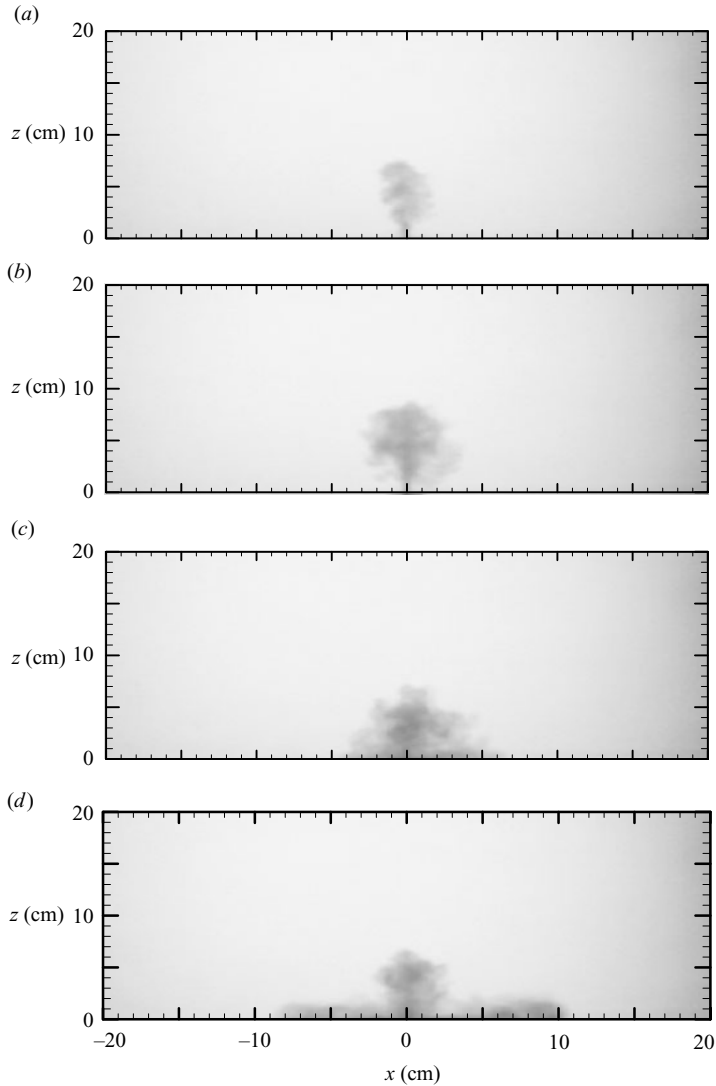
FIGURE 4. Snapshots of the one-layer experiment taken at (*a*) $t = 1$ s; (*b*) 3 s; (*c*) 5 s; (*d*) 8 s. The images have been flipped vertically for conceptual convenience.

Figure 6 shows snapshots of a two-layer experiment taken 2, 5, 10, 20 and 25 s after the experiment was started. In this experiment, the density difference between the fountain and the ambient fluid at the source was $|\rho_0 - \rho_1| = 0.001\,\mathrm{g\,cm^{-3}}$. The density difference between the two layers was $|\rho_1 - \rho_2| = 0.0012\,\mathrm{g\,cm^{-3}}$. The initial velocity was $w_0 = 23.9\,\mathrm{cm\,s^{-1}}$ and $H = 5$ cm. When the experiment begins, the fountain again increases in width as it entrains fluid from the surrounding ambient. It impinges upon the interface at $z = 5$ cm and penetrates through without noticeable change in structure (figure 6*a*).

After reaching the maximum height, the front of the fountain starts to broaden as more fluid is supplied from the source (figure 6*b*). It then returns downward, owing to its buoyancy excess, and collapses around the incident flow, similar to its behaviour in the one-layer case.
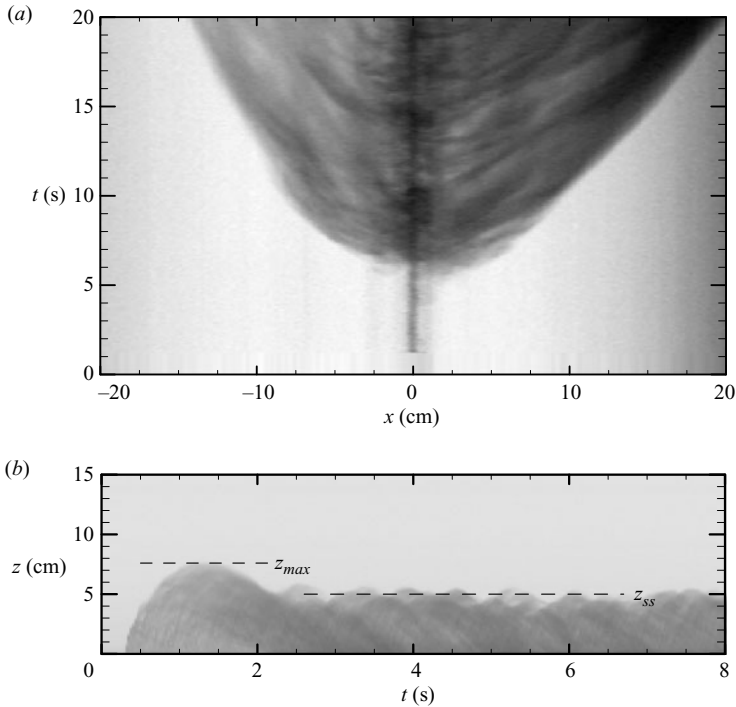
FIGURE 5. (*a*) Horizontal and (*b*) vertical time series for a one-layer experiment. The horizontal time series is constructed from a slice taken at $z = 0$ cm. The vertical time series is taken from a vertical slice through the source at $x = 0$ cm.

In this circumstance, however, the return flow becomes trapped at the interface and does not return to the source (figure 6*c*). At first, the return flow overshoots the height of the interface around the axis of the fountain before rising back to spread radially along the interface. The degree of overshoot is more or less pronounced, depending upon the experimental conditions. The process continues in a quasi-steady state (figure 6*d*). The spreading layer is observed to be thicker around the axis of the fountain and gradually reduces in thickness away from the axis (figure 6*e*).

Horizontal and vertical time series from this experiment are shown in figures 7(*a*) and 7(*b*), respectively. The former shows an intrusion moving with almost uniform radial speed toward the sidewalls of the tank. The time series is also observed to be symmetric about the source (situated at $x = 0$ cm). The measured positions of the maximum and steady-state heights are indicated on the vertical time series. Compared to the one-layer case, the average steady-state height is almost equal to the maximum height. This occurs because the return flow of the fountain intruded on the interface and so the distance over which the incident and return flows interact is reduced, thereby increasing the steady-state height.

5. Quantitative analyses

In this section, we quantitatively analyse the experimental results and compare them with theoretical predictions. The main aim is to characterize the various regimes of flow, to quantify the maximum penetration height in the two-layer ambient flow and to analyse the radial velocity of the resulting axisymmetric currents and intrusions.
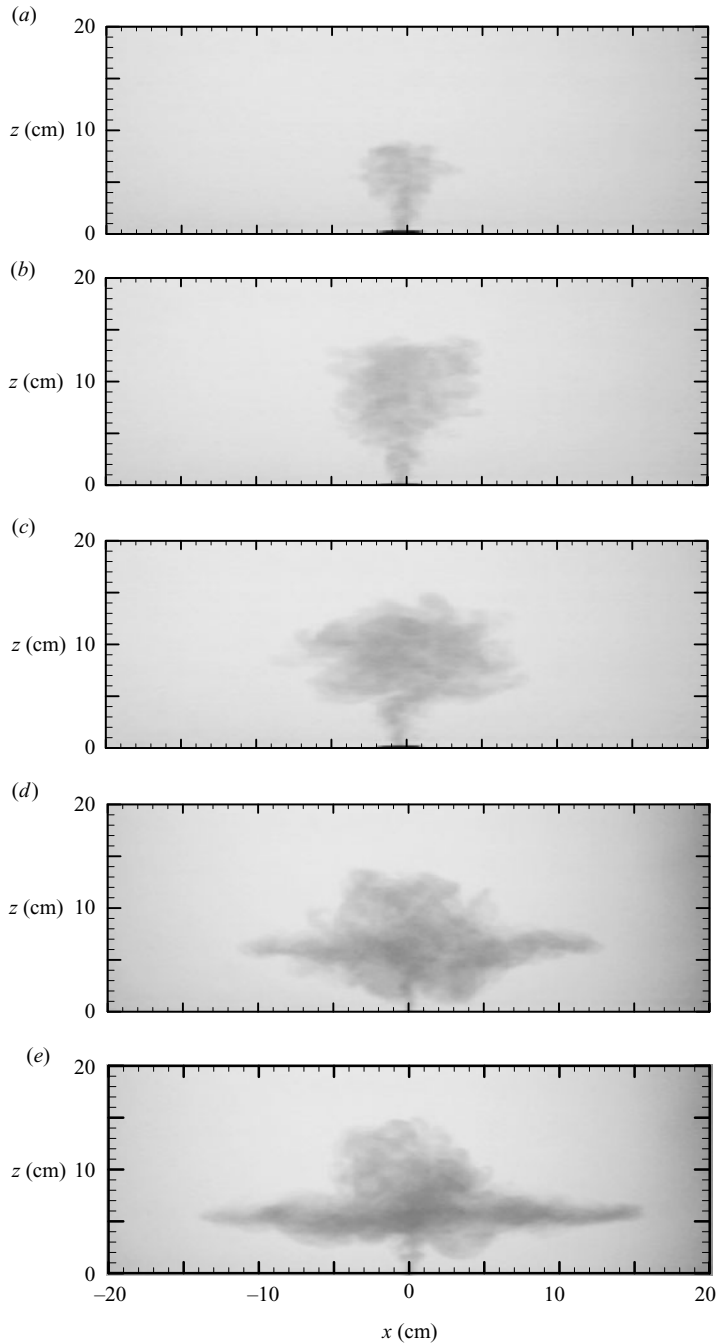
FIGURE 6. As in figure 4, but for snapshots of a two-layer experiment. (*a*) $t = 2$ s; (*b*) 5 s; (*c*) 10 s; (*d*) 20 s; (*e*) 25 s.

5.1. *Regime characterization*

The three regimes of flow observed in the experiments: in regime S, the return flow penetrates the interface, but returns vertically to the source; in regime I, the return flow intrudes at the interface; in regime B, a combination of both occurs.
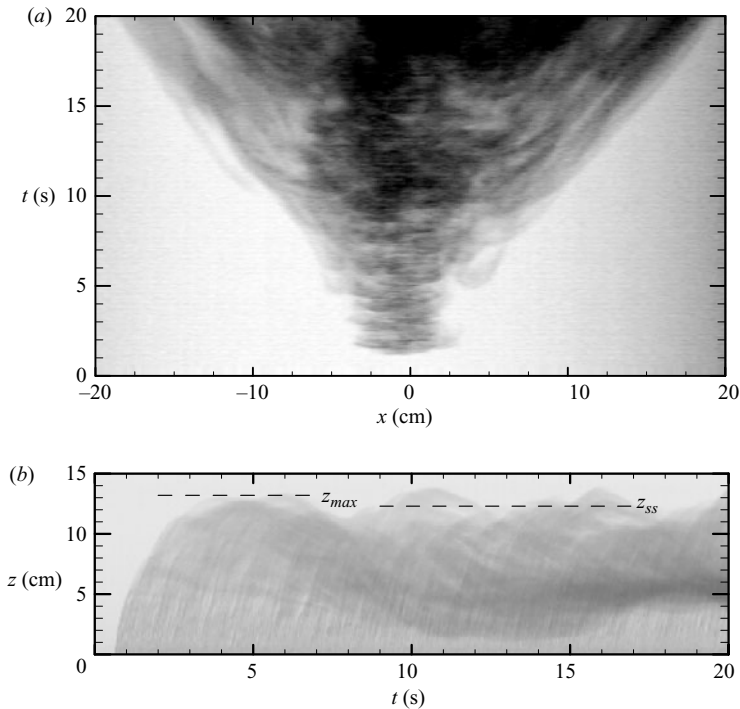
FIGURE 7. (*a*) As in figure 5, but for horizontal and (*b*) vertical time series for a two-layer experiment.

To classify the regimes of flow, we first considered an approach used by Bloomfield & Kerr (1998) to determine whether a fountain in a linearly stratified environment will spread at an intermediate level or spread at the source. In their method, the density of the fountain at the maximum height was first calculated and the height in the environment where fluid with this density would intrude was used as an estimate of the spreading height. To compare our results to those of Bloomfield & Kerr (1998), we calculated the density of the fountain at the maximum height, ρ_{max}, and compared it to the density in the first layer. In figure 8(*a*) we have plotted ρ_{max} against the density ρ_1. If ρ_{max} is larger (smaller, for fountains directed downward) than ρ_1, it is expected that the fountain will spread at the source. The experimental results show that this approach gives only a moderate classification of the regimes in the two-layer stratified case. About 28 % of the intrusions fell below the solid line in figure 8(*a*), predominantly for $H = 10$ cm cases. This probably means that it is possible to have sufficient mixing in the return flow by the time it reaches the interface, leading to interfacial intrusions. So a straightforward application of the diagnostic of Bloomfield & Kerr (1998) seems inappropriate for two-layer fluids because it does not account for the height of the interface, H.

A second classification of the regimes is shown in figure 8(*b*) where we have plotted the relative density differences $\theta = (\rho_2 - \rho_1)/(\rho_2 - \rho_0)$ against the relative maximum height z_{max}/H.

If $\theta \gtrsim 0.15$, figure 8(*b*) shows that intrusions form if $z_{max} \gtrsim 2H$. In which case the return flow entrains substantially less dense fluid from beyond the interface, making it lighter than the lower-layer fluid.
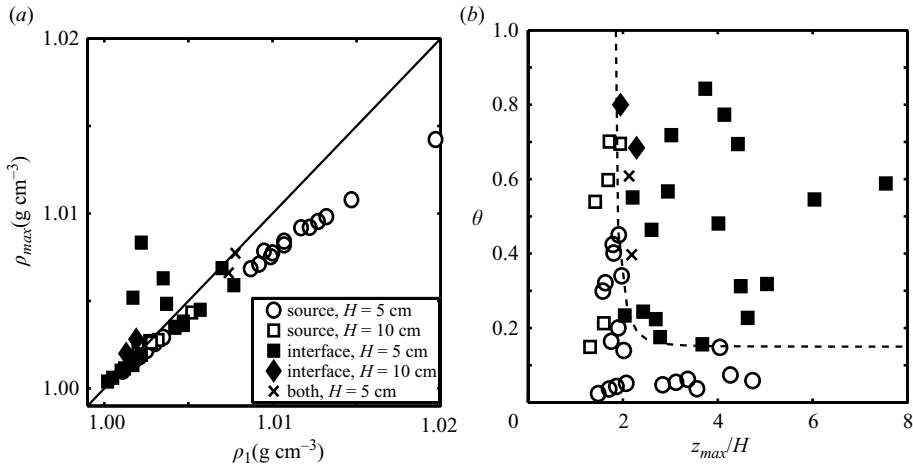
FIGURE 8. (*a*) Regime diagram following the method of Bloomfield & Kerr (1998); showing circumstances under which the return flow of a fountain spreads at the level of the source (open symbols), at the interface (closed symbols), or both. The solid line is expected to separate the open symbols from the closed symbols. (*b*) Regime diagram following our approach; the same symbols as (*a*). The dotted line represents an empirical formula that separates the two regimes and is given by (5.1).

If $\theta \lesssim 0.15$, the return flow reaches the source independent of the relative maximum height. In this case, the return flow also entrains less dense fluid from beyond the interface, but it is still heavier than the lower-layer fluid by the time it arrives at the interface. Likewise if $z_{max} \lesssim 2H$, the return flow always reaches the source because it is not sufficiently diluted by the ambient beyond the interface.

There were two experiments which resulted in regime B. They occurred for experiments with $z_{max} \approx 2H$. In these cases, the outer part of the return flow entrains more of the less dense fluid from beyond the interface than the inner part. The lighter outer part then begins to spread radially at the interface while the heavier inner part continues to fall to the source. The amount of fluid that intrudes at the interface may sometimes be smaller than the fluid that continues to the source.

The empirical function used to separate the intrusion and source outflow regimes is given by

$$\theta = 0.15 + \frac{1}{50(z_{max}/H - 1.5)^3}. \tag{5.1}$$

This is plotted as the dashed line in figure 8(*b*).

The second method of classification is therefore better for two-layer stratified fluids, as shown in figure 8(*b*). We note that the only calculation involved in this approach is that of z_{max} which is done from the source conditions (see (2.7)), unlike ρ_{max} which requires calculation of the axial parameters at the interface.

5.2. *Maximum height*

Figure 9(*a*) plots the experimentally measured values of $z_{max,2}$ and compares them with the theoretical prediction given by (2.12). There is good agreement in the data with a correlation of about 96 %. The results also compare well with the theoretical prediction of Abraham (1963) (see (2.13)).
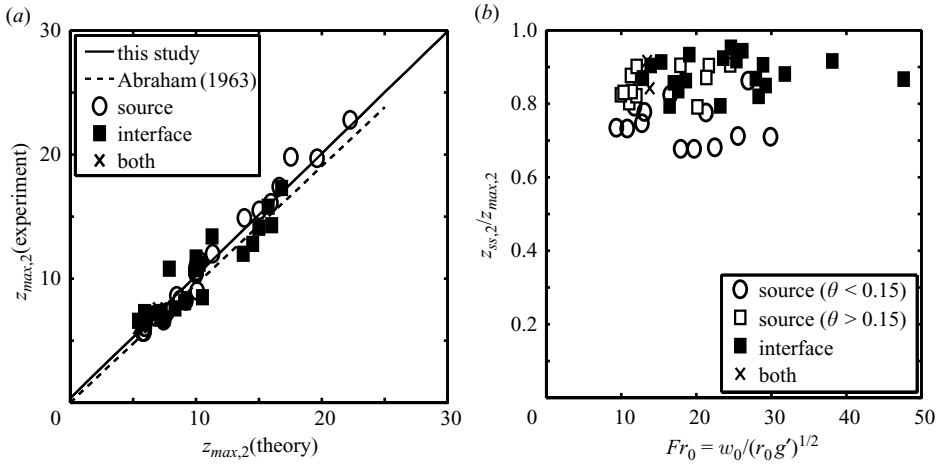
FIGURE 9. (*a*) The maximum penetration height and (*b*) the ratio of the steady-state height to the maximum height.

Figure 9(*b*) plots the ratio $z_{ss,2}/z_{max,2}$ against the source Froude number Fr_0. If $\theta < 0.15$, the average value of the ratio was found to be 0.74, which is comparable to the one-layer case. For the experiments with $\theta > 0.15$ and $z_{max} > 2H$ in which case the return flow intruded on the interface, the average value was 0.88. This occurs because the return flow penetrates little beyond the interface and so there is less interaction between the return and incident flows. If $\theta > 0.15$ and $z_{max} < 2H$, the average value was found to be 0.80, in this case the fountain penetrated little into the second layer.

Results of the ratio $z_{ss,2}/z_{max,2}$ are comparable to the findings of Bloomfield & Kerr (1998) for a fountain in a linearly stratified fluid where the average value of the ratio was found to be 0.93, also bigger than the value 0.70 for a fountain in a uniform ambient. This value is a little higher than our value of 0.88 for interfacial intrusions. This is probably because in the case of linearly stratified fluids, the fountain could intrude at intermediate heights which are higher than the equivalent heights of the two-layer interface. This means that, effectively, the distance over which the upflow and downflow interact is even shorter in a linearly stratified ambient, leading to a higher value of the ratio.

5.3. *Radial source and intrusion speeds*

We measured the initial velocity of the radially spreading currents by taking the slope near $x \approx R_f$ of horizontal time series as shown, for example, in figure 10.

Measurements of the time and distance from the horizontal time series determined how the position of the front scales with time near $x = R_f$. Figure 11 shows some typical log–log plots of distance against time used to determine the scaling relationship. The experiments showed steady-state ($R \sim t$) and inertia–buoyancy ($R \sim t^{3/4}$) regimes in the flow.

To gain a better understanding of the starting flow regimes, we defined a critical Froude number to characterize the competing effects of momentum and buoyancy in the return flow at the point of entry of the current into the ambient. In the case of the flows that returned to the source, the Froude number is defined by

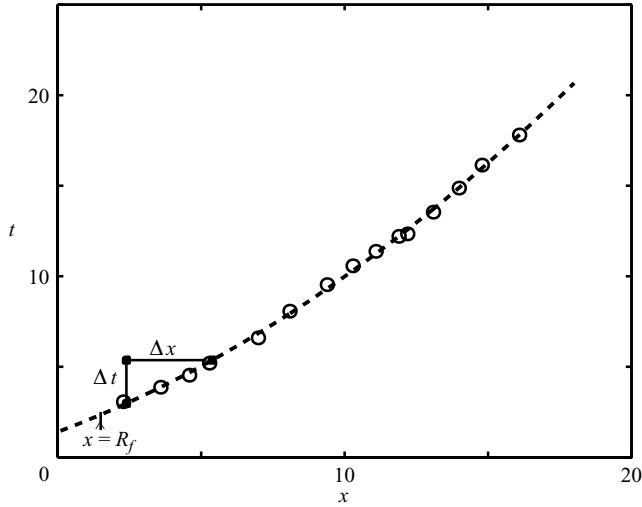$$Fr_s = w_{ret}/(g'_{ret}z_{max,2})^{1/2}, \tag{5.2}$$

FIGURE 10. Typical approach of calculating the initial spreading speeds with $\Delta x \approx R_f$ (experiment with $|\rho_1 - \rho_0| = 0.0202$, $|\rho_2 - \rho_1| = 0.0005$, $H = 5$ cm, $w_0 = 26.26$ cm s^{-1}). $\bigcirc$, experimental data; - - -, fitted line.
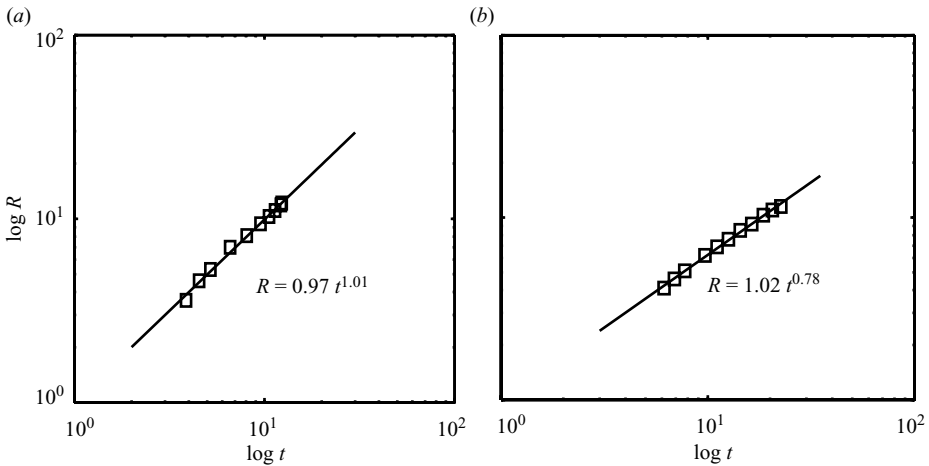

FIGURE 11. Typical initial growth relationships between the radial distance and time, indicating (a) $R \sim t$ (experiment with $|\rho_1 - \rho_0| = 0.0022$, $|\rho_2 - \rho_1| = 0.005$, $H = 5$ cm, $w_0 = 25.95$ cm s^{-1}), and (b) $R \sim t^{3/4}$ (experiment with $|\rho_1 - \rho_0| = 0.0202$, $|\rho_2 - \rho_1| = 0.0005$, $H = 5$ cm, and $w_0 = 26.26$ cm s^{-1}). $\square$, experimental data; —, fitted line.

where $g'_{ret} = (F_0 + F_i)/Q_{st}$ is the reduced gravity of the return flow at the level of the source. In the case of the interfacial flows, the Froude number is similarly defined by

$$Fr_i = w_{ret,i}/(g'_{ret,i} z_{max,2})^{1/2}, \tag{5.3}$$

where $g'_{ret,i}$ is the reduced gravity of the return flow at the interface. Figure 12 gives an approximate classification of these regimes. It shows that the power law relation $R \sim t^\alpha$ with $\alpha \approx 0.75$ occurs for smaller values of the Froude number ($Fr_s < 0.25$ and $Fr_i < 0.4$). In this case, the initial flow is driven purely by buoyancy forces while
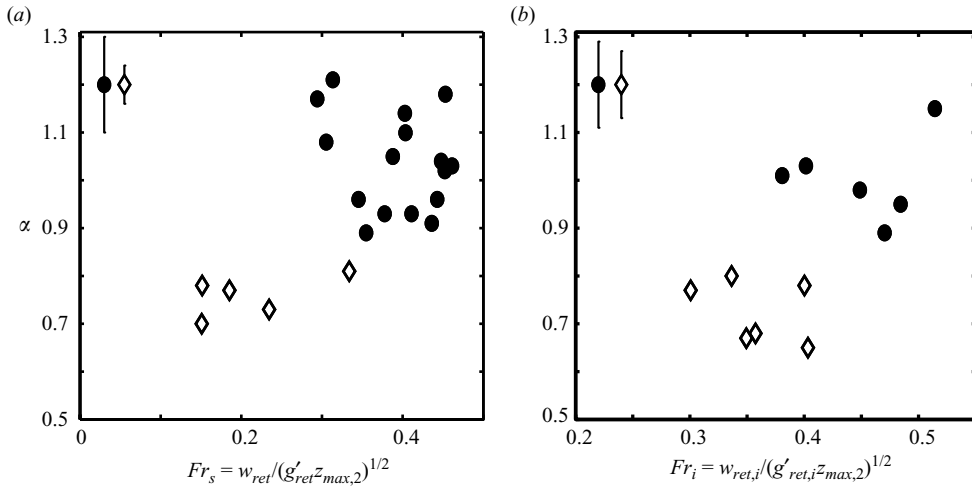
FIGURE 12. Characterizing the initial power-law behaviour, $R \sim t^{\alpha}$, using a defined radial Froude number for the (a) surface flows, and (b) interfacial flows. $\diamond$, $\alpha \approx 0.75$; $\bullet$, $\alpha \approx 1$. Typical errors are indicated in the top left-hand corner of both plots.
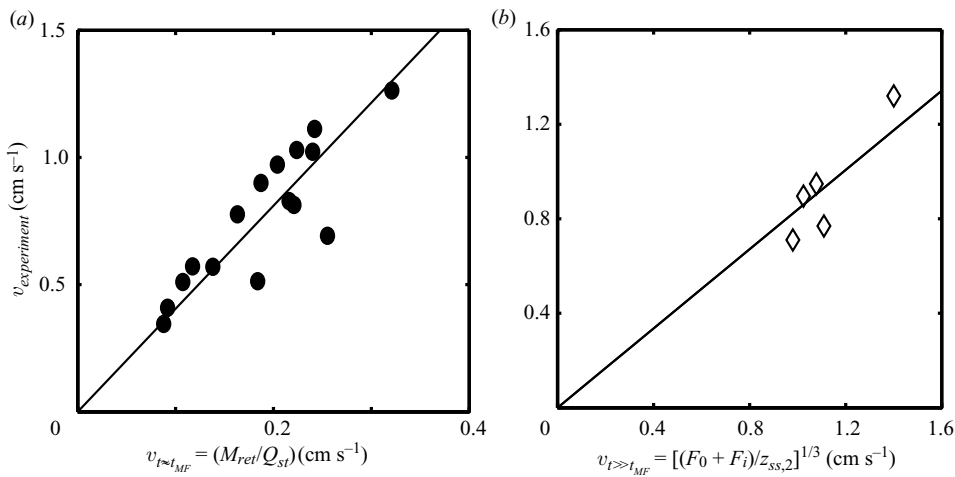

FIGURE 13. Radial initial surface spreading velocities for (a) $R \sim t$, and (b) $R \sim t^{3/4}$.

for larger values of the Froude number ($Fr_s > 0.25$ and $Fr_i > 0.4$), both momentum and buoyancy play a role in the initial flow, giving rise to a power-law exponent $\alpha \approx 1.0$.

If instabilities develop in the flow, causing the fountain to tilt initially to one side of its vertical axis, then these scaling relationships may be violated. This was also observed to occur if, in the case of the intrusions, there was a very strong overshoot of the return flow before rising back to spread along the interface. The velocity data used to determine the experimental constants in the theory do not include those experiments.

5.3.1. *Source-spreading speeds*

Figure 13 plots the measured speeds of the radially propagating currents at the source compared with the theoretical estimates of (3.17) and (3.19). We see that there
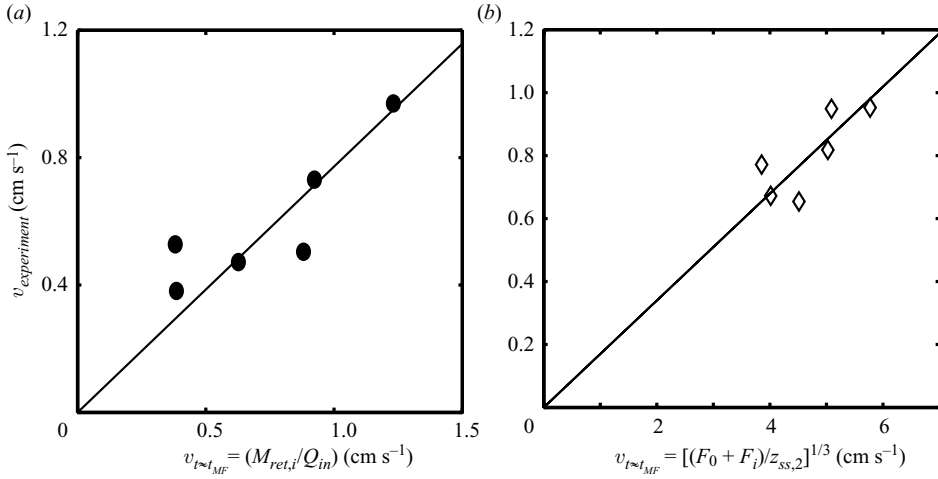
FIGURE 14. Radial initial intrusion velocities for (a) $R \sim t$, and (b) $R \sim t^{3/4}$.

is fairly good agreement between the theory and the measurement. The theoretical equations for these two regimes then become

$$v_{t \approx t_{MF}} = (4.10 \pm 0.14) \left(\frac{M_{ret}}{Q_{st}} \right), \tag{5.4}$$

$$v_{t \gg t_{MF}} = (0.84 \pm 0.14) \left(\frac{F_0 + F_i}{z_{ss,2}} \right)^{1/3}. \tag{5.5}$$

The regimes of flow in this case are the constant-velocity regime ($R \sim t^\alpha$ with $\alpha = 1.0 \pm 0.10$) and the inertia–buoyancy regime ($\alpha = 0.75 \pm 0.04$).

5.3.2. *Intrusion speeds*

Figure 14 plots the measured intrusion speeds against the theoretical estimates of (3.21) and (3.23). The theoretical equations for these two regimes then become

$$v_{t \approx t_{MF}} = (0.77 \pm 0.15) \left(\frac{M_{ret,i}}{Q_{in}} \right), \tag{5.6}$$

$$v_{t \gg t_{MF}} = (0.17 \pm 0.09) \left(\frac{F_0 + F_i}{z_{ss,2}} \right)^{1/3}. \tag{5.7}$$

The regimes of flow in this case are the constant-velocity regime ($\alpha = 1.0 \pm 0.09$) and the inertia–buoyancy regime ($\alpha = 0.75 \pm 0.07$).

We observe that the proportionality contants in the interfacial intrusions are much smaller than the constants in the source-spreading case. This is probably caused by higher retarding forces exerted by the two fluid layers on the interfacial currents unlike the currents at the source which propagate on the interface between air and liquid and therefore experienced a much smaller resisting force from the ambient.

6. Summary and conclusions

We have classified the regimes of flow that result when an axisymmetric turbulent fountain is discharged into a two-layer ambient. The classification was made using the empirically determined parameter, $\theta = (\rho_2 - \rho_1)/(\rho_2 - \rho_0)$, and the relative maximum

height, z_{max}/H. The results show that if $z_{max} \lesssim 2H$, the return flow will go back to the source irrespective of the value of θ. However, if $z_{max} \gtrsim 2H$, the return flow will collapse and spread radially at the interface if $\theta \gtrsim 0.15$.

We found good agreement between theory and experiment for the maximum vertical penetration height. In the case of flows which returned to the source, the ratio of the quasi-steady-state height to the maximum height, $z_{ss,2}/z_{max,2}$, was found to depend on whether the return flow went back to the source or collapsed at the interface. The ratio is closer to unity ($z_{ss,2}/z_{max,2} \approx 1.0$) for intrusions because the return flow does not retard the incident flow in the ambient near the source.

Radial currents that result from the return flow of a fountain spreading at the source or interface either at constant velocity (being driven by both the radial components of momentum and buoyancy) or spreading as $R \sim t^{3/4}$ (being driven by buoyancy forces alone). These regimes are distinguished by a critical Froude number $Fr_s \approx 0.25$ or $Fr_i \approx 0.4$.

In the future, we wish to extend the ideas developed in this study to the case of the dispersion of pollutants from flares which disperse in the presence of an atmospheric inversion.

Appendix A. Virtual origin correction

Morton (1959b) predicted the virtual origin for a negatively buoyant forced plume to occur at

$$z_v = 10^{1/2} \gamma^{3/2} L_m \int_{1/\gamma}^{1} (1 - \tau^5)^{-1/2} \tau^3 \mathrm{d}t, \tag{A 1}$$

where

$$L_m = \frac{1}{\left(2^{3/2} \tilde{\alpha}^{1/2} \pi^{1/4} \lambda\right)} \frac{M_0^{3/4}}{|F_0|^{1/2}}, \quad \Gamma = \frac{5\lambda^2}{4\tilde{\alpha}\pi^{1/2}} \frac{|F_0| Q_0^2}{M_0^{5/2}}, \quad \gamma = (1 - \Gamma)^{1/5}.$$

The entrainment constant is $\tilde{\alpha} = 0.085$ for fountains (Bloomfield & Kerr 2000) and $\lambda = 1$ for top-hat profiles.

Appendix B. Scaling analyses: radial intrusion in a two-layer environment

Consider an axisymmetric intrusion of density ρ_{in} from a source of constant volume flux Q_{in} into a two-layer environment with a top layer of density ρ_1 and a lower layer of density ρ_2. Let h be the height of the intrusion at time t and H be the distance of the interface from the surface (figure 15). We assume small density differences between the intrusion and the ambient and neglect surface-tension effects.

The conservation of volume relation is given by

$$Q_{in}t \sim R^2 h, \tag{B 1}$$

where R is the position of the front at time t. The pressure distribution within the intrusion can be obtain from the hydrostatic equation ($\mathrm{d}p/\mathrm{d}z = -\rho_{in}g$) such that

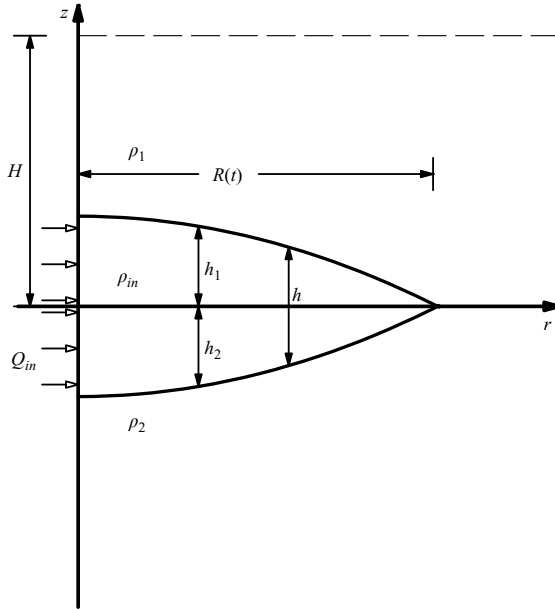$$p = p_0 - \rho_{in}gz + g(\rho_{in} - \rho_1)h_1, \tag{B 2}$$

FIGURE 15. Schematic of intrusion into a two-layer environment.

where $p_0 = \rho_1 gH$. A relation between h_1 and h is obtained via a hydrostatic balance (Timothy 1977):

$$h_1 = \left(\frac{\rho_2 - \rho_{in}}{\rho_2 - \rho_1} \right) h. \tag{B3}$$

Thus, from (B2), we find the pressure distribution

$$p = p_0 - \rho_{in} gz + \rho_{in} \varepsilon g'_{in} h, \tag{B4}$$

where $\varepsilon = (\rho_2 - \rho_{in})/(\rho_2 - \rho_1)$ and $g'_{in} = g(\rho_{in} - \rho_1)/\rho_{in}$. The radial pressure gradient is therefore given by

$$\frac{\partial p}{\partial r} = \rho_{in} \varepsilon g'_{in} \frac{\partial h}{\partial r}. \tag{B5}$$

At the interface, $z = 0$, the pressure scales as $p \sim \rho_{in} \varepsilon g'_{in} h$ and so the horizontal driving pressure force should scale as the product of the pressure and the cross-sectional area:

$$F_p \sim \rho_{in} \varepsilon g'_{in} Rh^2. \tag{B6}$$

In the inertia–buoyancy regime, the opposing force is the inertia force, F_{in}, which scales as the product of the mass and acceleration:

$$F_{in} \sim \rho_{in} hR^3/t^2. \tag{B7}$$

Balancing (B6) and (B7) and using (B1), we obtain

$$R(t) \sim (\varepsilon g'_{in} Q_{in})^{1/4} t^{3/4}. \tag{B8}$$

REFERENCES

ABRAHAM, G. 1963 *Jet diffusion in stagnant ambient fluid*. Delft Hydraulics Laboratory, Publication 29.

BAINES, W. & CHU, V. 1996 *'Jets and Plumes' in Environmental Hydraulics,* chap. 2. Kluwer.

BAINES, W., TURNER, J. & CAMPBELL, I. 1990 Turbulent fountains in an open chamber. *J. Fluid Mech.* **212**, 557–592.

BLOOMFIELD, L. & KERR, R. 1998 Turbulent fountains in a stratified fluid. *J. Fluid Mech.* **358**, 335–356.

BLOOMFIELD, L. & KERR, R. 2000 A theoretical model of a turbulent fountain. *J. Fluid Mech.* **424**, 197–216.

BRITTER, R. 1979 The spread of a negatively buoyant plume in a calm environment. *Atmos. Environ.* **13**, 1241–1247.

BRITTER, R. 1989 Atmospheric dispersion of dense gases. *Annu. Rev. Fluid Mech.* **21**, 317–344.

CHEN, J.-C. 1980 Studies on gravitational spreading currents. PhD thesis, California Institute of Technology.

DAVIERO, G., ROBERTS, J. & MILE, K. 2001 Refractive index matching in large-scale experiments. *Exps. Fluids* **31**, 119–126.

FISCHER, H., LIST, E., IMBERGER, J. & BROOKS, N. 1979 *Mixing in Inland and Coastal Waters*. Academic.

FRIEDMAN, P. & KATZ, J. 2000 Rise height for negatively buoyant fountains and depth of penetration for negatively buoyant jets impinging an interface. Trans. ASME I: *J. Fluids Engng* **122**, 779–782.

KAPOOR, K. & JALURIA, Y. 1993 Penetrative convection of a plane turbulent wall jet in a two-layer thermally stable environment: a problem in enclosure fires. *Intl J. Heat Mass Transfer* **36**, 155–167.

KOTSOVINOS, N. 2000 Axisymmetric submerged intrusion in stratified fluid. *J. Hydrau Engng ASCE* **126**, 446–456.

LEE, J. & CHU, V. 2003 *Turbulent Buoyant Jets and Plumes: A Langrangian Approach*. Kluwer.

LIN, Y. & LINDEN, P. 2005a A model for an under floor air distribution system. *Energy and Buildings* **37**, 399–409.

LIN, Y. & LINDEN, P. 2005b The entrainment due to a turbulent fountain at a density interface. *J. Fluid Mech.* **542**, 25–52.

LIST, E. 1982 Turbulent jets and plumes. *Annu. Rev. Fluid Mech.* **14**, 189–212.

LISTER, J. & KERR, R. 1989 Viscous gravity currents at a fluid interface. *J. Fluid Mech.* **203**, 215–249.

MCDOUGALL, T. 1981 Negatively buoyant vertical jets. *Tellus* **33**, 313–320.

MELLOR, G. 1996 *Introduction to Physical Oceanography*. Springer.

MIZUSHINA, T., OGINO, F., TAKEUCHI, H. & IKAWA, H. 1982 An experimental study of vertical turbulent jet with negative buoyancy. *Warme and Stoffubertragung (Thermo and Fluid Dynamics)* **16**, 15–21.

MORTON, R. 1959a The ascent of turbulent forced plumes in a calm atmosphere. *Intl J. Air Pollution* **1**, 184–197.

MORTON, R. 1959b Forced plumes. *J. Fluid Mech.* **5**, 151–163.

MORTON, R., TAYLOR, G. & TURNER, J. 1956 Turbulent gravitational convection from maintained and instantaneous sources. *Proc. R. Soc. Lond.* A **234**, 1–23.

NOUTSOPOULOS, G. & NANOU, K. 1986 The round jet in a two-layer stratified ambient. *Proc. Intl Symp. on Buoyant Flows: Athens-Greece* vol. 1–5, 165–183.

PRIESTLEY, C. & BALL, F. 1955 Continuous convection from an isolated source of heat. *Q. J. R. Met. Soc.* **81**, 144–156.

RAWN, A., BOWERMAN, F. & BROOKS, N. 1960 Diffusers for disposal of sewage in sea water. *J. Sanitary Engng Div. Proc. ASCE* **86**, 65–105.

RODI, W. 1982 *Turbulent Buoyant Jets and Plumes*. Pergamon.

SCORER, R. 1959 The behaviour of chimney plumes. *Intl J. Air Pollution* **1**, 198–220.

SEBAN, R., BEHNIA, M. & ABREU, K. 1978 Temperatures in a heated air jet discharged downward. *Intl J. Heat Mass Transfer* **21**, 1453–1458.

SHY, S. 1995 Mixing dynamics of jet interaction with a sharp density interface. *Expl Thermal Fluid Sci.* **10**, 355–369.

TIMOTHY, W. 1977 Density currents and their applications. *J. Hydraul. Div.* **103**, HY5, 543–555.

TURNER, J. 1966 Jets and plumes with negative or reversing buoyancy. *J. Fluid Mech.* **26**, 779–792.

TURNER, J. 1973 *Buoyancy Effects in Fluids*. Cambridge University Press.